Available online at www.sciencedirect.com
ScienceDirect
Nuclear Instruments and Methods in Physics Research B 266 (2008) 4092–4096
NIM B
Beam Interactions with Materials & Atoms
www.elsevier.com/locate/nimb

RIB production by photofission in the framework of the ALTO project: First experimental measurements and Monte-Carlo simulations

M. Cheikh Mhamed *, S. Essabaa, C. Lau, M. Lebois, B. Roussière, M. Ducourtieux, S. Franchoo, D. Guillemaud Mueller, F. Ibrahim, J.F. LeDu, J. Lesrel, A.C. Mueller, M. Raynaud, A. Said, D. Verney, S. Wurth

Institut de Physique Nucléaire, IN2P3-CNRS/Université Paris-Sud, F-91406 Orsay Cedex, France

Available online 11 June 2008

Abstract

The ALTO facility (Accélérateur Linéaire auprès du Tandem d'Orsay) has been built and is now under commissioning. The facility is intended for the production of low energy neutron-rich ion-beams by ISOL technique. This will open new perspectives in the study of nuclei very far from the valley of stability. Neutron-rich nuclei are produced by photofission in a thick uranium carbide target (UC_x) using a 10 μA, 50 MeV electron beam. The target is the same as that already had been used on the previous deuteron based fission ISOL setup (PARRNE [F. Clapier et al., Phys. Rev. ST-AB (1998) 013501.]). The intended nominal fission rate is about 10^{11} fissions/s. We have studied the adequacy of a thick carbide uranium target to produce neutron-rich nuclei by photofission by means of Monte-Carlo simulations. We present the production rates in the target and after extraction and mass separation steps. The results from Monte-Carlo simulations are compared to experimental data either with the ALTO facility (in the first step of commissioning, i.e. 100 nA of the electron beam current intensity), or with fast-neutron-induced fission generated from a 26 MeV deuteron beam. The results obtained support the suitability of FLUKA simulation code used to describe all the photofission process with an electron beam energy of 50 MeV.

PACS: 25.20.−x; 24.10.Lx; 29.25.−t; 29.25.Rm

Keywords: Photofission; Monte-Carlo simulations; Radioactive ion beams; Production Yields; Uranium carbide targets; ISOL technique

1. The ALTO facility

The ALTO facility [2] has been built and now is under commissioning. The electron driver can deliver a primary beam at the energy of 50 MeV with a nominal intensity of 10 μA. The main characteristics of the Linac are presented in [3,4].

The accelerated 50 MeV electron beam is transported and focused on a thick $^{238}UC_x$ target ISOLDE-type. Fission fragments diffuse out of the target at high temperature and effuse towards the ion source to be ionized with a charge state 1^+. Produced ions are extracted and accelerated with a 30 kV voltage towards the on-line isotope separator PARRNe2. An overview layout of the ALTO facility is presented in Fig. 1.

The ALTO target is similar to that used during previous experiments with a deuteron beam (Fig. 2) in order to allow a direct comparison. It is a thick target of uranium carbide ($^{238}UC_x$) made by an assembly of disks of 14 mm diameter, 1 mm thick along a length of 140 mm and put in a graphite container. It contains 60.8 g of ^{238}U and the apparent density is about 3.2 g/cm^3. The fabrication process is similar to that used at CERN for thick targets [5,6]. The target can be heated at a temperature up to 2100 °C for fast release of the produced radioactive elements.

For ALTO commissioning and in order to have comparable operational conditions with previous PARRNe

* Corresponding author. Tel.: +33 1 69 15 62 25; fax: +33 1 69 15 51 08.
E-mail address: cheikh@ipno.in2p3.fr (M. Cheikh Mhamed).

0168-583X/$ - see front matter © 2008 Elsevier B.V. All rights reserved.
doi:10.1016/j.nimb.2008.05.127

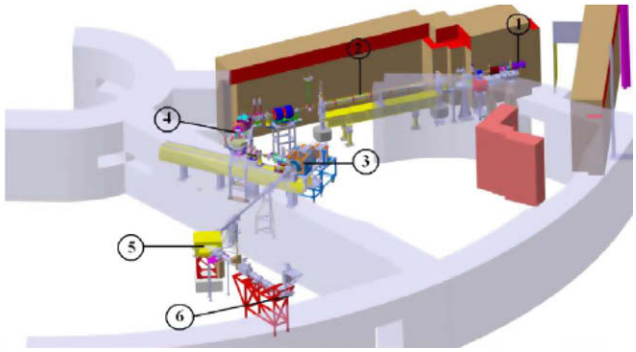

Fig. 1. Layout of ALTO associated to the online isotope separator PARRNe2: (1) electron gun, (2) accelerating section, (3) target and ion source, (4) beam line, (5) mass separator, and (6) detection system.

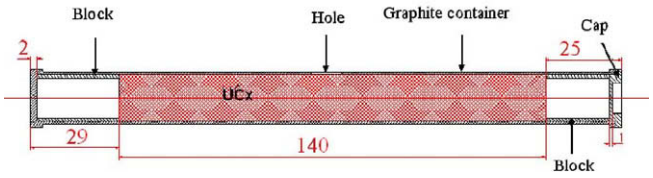

Fig. 2. Structure of the ALTO target. The cap is used to trap the target in the container. By means of two blocks, the 14 cm-long target is put in the middle of a 20 cm tantalum oven so as to have an homogenous heating temperature. The fission fragments can only escape by the central hole.

experiments, a FEBIAD ion source [7–9] is associated to the UC_x target. This choice is based on the capability of the ion source to produce a wide variety of isotope beams, which allows us to get a maximum of data on RIB that can be produced at ALTO. As a consequence, this high temperature ion source is the least selective: one of the most penalizing criteria in terms of radioprotection.

However, it is envisaged to use other types of sources for ALTO such as the IRENA (Ionization by Radial Electron Neat Adaptation) [10,11] ion source and the RILIS (Resonance Ionization Laser Ion Source) [12]. Furthermore, ALTO is planned to be in part a "TIS" (Target Ion Source) R&D facility for SPIRAL2 and EURISOL, so all ion sources considered in these projects could be tested at ALTO.

2. RIB production by photofission

We have performed a full study of the adequacy of the target for the production of radioactive neutron rich nuclei by photofission. For this purpose, we have used the FLUKA [13,14] Monte-Carlo code. We assume that the 50 MeV electron beam hits directly the UC_x target, that means the photons of bremsstrahlung are generated directly inside the UC_x target.

In Fig. 3 we present the spatial distribution of the incident electrons inside the target. From this distribution we can notice that electrons are slowed down quickly in the beginning of the target and almost totality of the energy is lost after a penetration distance of ~2.65 cm. The electromagnetic shower is initiated in this region. Moreover the total power deposition simulations in the target show a maximum hot spot of ~37 W/cm^3 located at the beginning of the target [4].

The spatial fission distribution in the target obtained in Fig. 4 shows that fission distribution in the target is not homogenous and the maximum fission rate is located in the beginning of the target too. The saturation of the fission rate is reached after a penetration length about 14 cm and the accumulated fission rate given by simulation is about 8×10^{10} fissions/s (Fig. 5). In the frame of this

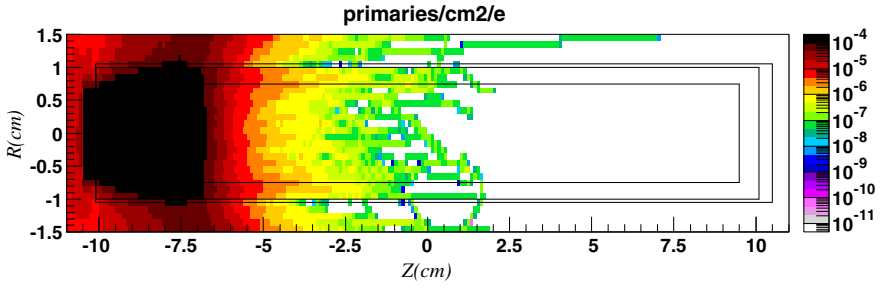

Fig. 3. Spatial distribution of the incident electrons (primary electrons) (primaries/cm^2/e) in the ALTO target with 50 MeV incident electron beam.

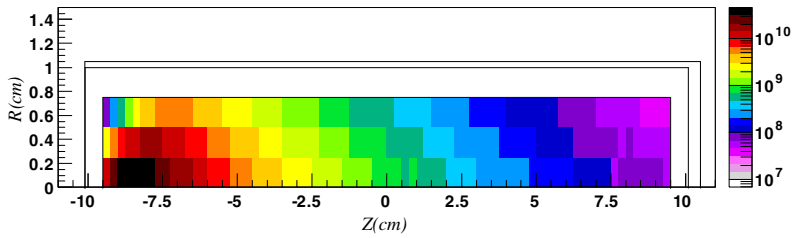

Fig. 4. Spatial distribution of the fission density (fissions/cm^3/s) in the ALTO target for 50 MeV and 10 μA incident electron beam.

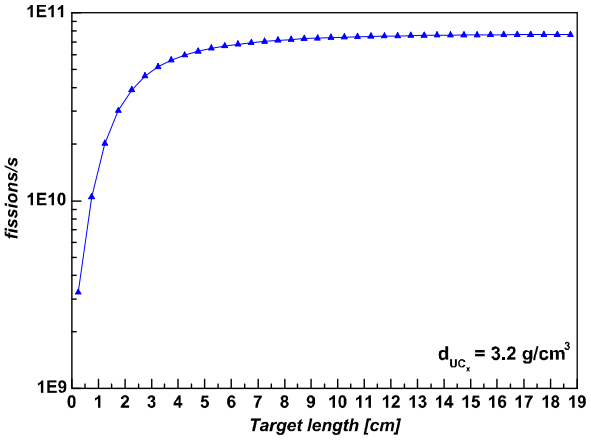

Fig. 5. Accumulated fission rate according to the target length for 50 MeV and 10 μA incident electron beam.

work, the contribution of photoneutrons to the fission rate has been estimated, by means of FLUKA Monte-Carlo simulations, to be two orders of magnitude lower than photon contribution [4].

2.1. In-target production

Literature is poor concerning experimental data of photofission and given production yields are often not complete. We have estimated the in-target production by means of the RESNUCLEI module of FLUKA and results have been compared to the cumulative experimental production yields given by Jacobs et al. [15] for 30 MeV and 70 MeV electron beams. The simulation results presented in this paper are performed with 10 millions electron histories. All nuclear data needed in FLUKA for presented simulations were taken from ENDFB6-R8 libraries.

In Fig. 6 we compare this situation with the experimental cumulative production yields given by Jacobs et al. for 30 MeV and 70 MeV electron beams. All data have been normalized proportionately to the fission rate expected

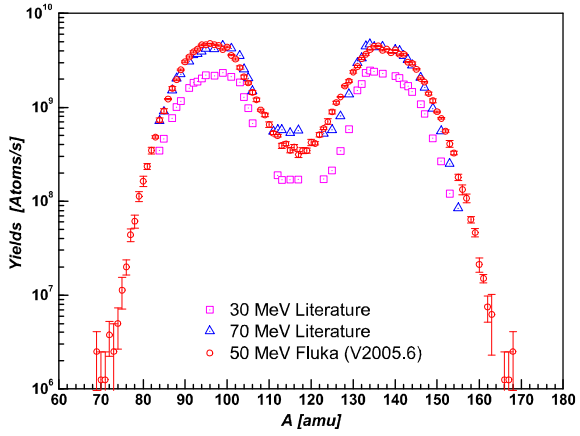

Fig. 6. Photofission mass distributions for electron beam energies of 30 MeV [15], 50 MeV (simulations) and 70 MeV [15].

with ALTO and using uranium fission yield data from [16]. One can notice the rising of symmetrical fission with increasing electron energy. However for these electron energies fission remains asymmetrical with two mass peaks around 95 uma and 135 uma. The curves corresponding to 50 MeV and 70 MeV nearly overlap. The reason of this is the saturation of the uranium fission yield curve as a function of the electron energy around 50 MeV [16].

2.2. On-line RIB production

During the first commissioning step, the electron driver intensity has been limited at 100 nA. The commissioning program of ALTO includes five steps aiming to reach smoothly the nominal current intensity of the accelerator. These steps correspond to 100 nA, 500 nA, 1 μA, 5 μA and 10 μA of the current electron beam intensity.

For 100 nA the production rates are expected to be similar to that obtained with 26 MeV and 1 μA deuteron beam in the previous PARRNe experiment [17]. To allow a direct comparison with the results obtained in this previous experiment we have used the same target-ion source system (c.f Section 1).

In this paper we present only the results obtained for isotopic chains of rare gases Krypton (Kr) and Xenon (Xe), metallic isotopes of Tin (Sn), and halogen isotopes of Iodine (I). The separated beam is collected on a mylar/aluminium tape during a given collection time depending on the half-life of the studied isotope. Two counting stations are gripped with plastic and Ge(HP) detectors to perform β and γ spectroscopy measurements. One of the counting stations is located at the collection point. More details on the experimental setup and on the yield determination can be found in [18].

Production yields of Kr, Xe, I and Sn have been also estimated by means of FLUKA simulations. The RESNUCLEI FLUKA module gives the in-target production for all species produced in the UC_x target. In order to estimate the production yields on the mylar tape, we should use the following Eq. (1):

$$I_{\text{beam}} = \sigma \times \Phi \times N \times \epsilon \tag{1}$$

I_{beam} is the intensity of the focused beam at the collection point, σ: production cross section, Φ: the primary beam intensity, N: the usable target thickness and $\epsilon = \varepsilon_r \times \varepsilon_{\text{ion}} \times \varepsilon_{\text{tr}}$ is the global efficiency value. ϵ is defined by the product of the release efficiency (ε_r), ionisation efficiency (ε_{ion}) of the radioactive element of interest and the transport efficiency (ε_{tr}) of the mass-separator. For PARRNe2 ε_{tr} is about 80%. Ionisation efficiencies for Kr, Xe, Sn using a FEBIAD ion source type are, respectively of 5%, 5% and 6% [19,20], whereas for I the ionisation efficiency is estimated to be about 10%. Finally, release efficiencies are determined depending on whether effusion process or diffusion process is the most predominant. Release times for these elements have been determined experimentally during previous PARRNe experiments [21,17].

Knowing the half-life $T_{1/2}$ and the release time T_R release efficiency can be determined either by Eq. (2) for effusion process or by Eq. (3) for diffusion process and assuming spherical shape of grains which form the target.

$$\varepsilon_r = \frac{T_{1/2}}{T_{1/2} + T_R} \tag{2}$$

$$\varepsilon_r = \frac{3\left(\sqrt{\pi^2 \frac{T_R}{T_{1/2}}} \times \coth\left(\sqrt{\pi^2 \frac{T_R}{T_{1/2}}}\right) - 1\right)}{\pi^2 \frac{T_R}{T_{1/2}}} \tag{3}$$

A summary of the dominant release process and the release times measured at PARRNe is given for isotopes of Kr, Xe, Sn and I in the following Table 1.

2.2.1. Results and discussions

Let's notice that estimated values are obtained from independent yields while the measured ones include the feeding from the β – *decay* inside the target. Preliminary comparison between FLUKA simulations and the experimental results have been presented in [18].

2.2.1.1. Isotopic chain of Kr. Beam intensities of Krypton isotopes are presented in Fig. 7. PARRNe and ALTO experimental measurements are in good agreement. Monte-Carlo calculation fully matches these results, except for ^{94}Kr. In that case, the measured yield is a rough estimation since the absolute γ intensity of the γ-*ray* used in the production determination is not known and has been assumed to be 50%. For short-lived elements independent production yields and cumulative production yields are practically identical. However, due to the use of a thick target accumulated productions yield become more important for long-lived elements. This effect grows with the rising of the half-life of the radioactive elements. Such effect can be seen for ^{89}Kr ($T_{1/2} = 3.18$ mn), ^{88}Kr ($T_{1/2} = 2.84$ h) and ^{87}Kr ($T_{1/2} = 76.3$ mn).

Table 1
Release properties of Kr, Xe, Sn and Iodine isotopes [21]

Isotope	Release process	T_R (s)
Kr	Diffusion	11 ± 3
Xe	Diffusion	21 ± 6
Sn	Effusion	55 ± 10
I	Diffusion	17 ± 6

2.2.1.2. Isotopic chain of Xe. Beam intensities of Xenon isotopes are reported in Fig. 8. We observe a very good accuracy of the FLUKA simulation for short-lived elements up to ^{141}Xe. The absolute intensity of the γ-*rays* signing the decay of ^{142}Xe and ^{143}Xe are not known. The yields have been estimated assuming absolute intensity of the strongest γ-*rays* equal to 50% and this can explain the discrepancy between the measured and estimated values.

As we have seen in the case of the isotopic chain of Kr, cumulative production yields are also important for the ^{137}Xe, ^{138}Xe and ^{139}Xe [24], but this effect is not visible in Fig. 8. In fact, for a heating temperature of the target from 1500 °C up to 2000 °C release times of Br isotopes which beta decay to Kr isotopes are much more important (a nearly factor of 10) than the release times of Iodine isotopes which beta decay to Xe isotopes [21–23]. In addition, the collection time on the mylar type in our experimental conditions was 10–20 s. This therefore implies that Br isotopes have more chance than Iodine isotopes to feed its daughters: in this case Kr isotopes.

2.2.1.3. Isotopic chain of Sn. In Fig. 9 we represent the production yields obtained for Tin isotopes. Measurements obtained with ALTO are in good agreement with PARRNe. These experimental values are well reproduced by the FLUKA simulations. However the odd–even effect due to the cold fission phenomena in photofission is slightly underestimated in the FLUKA simulations.

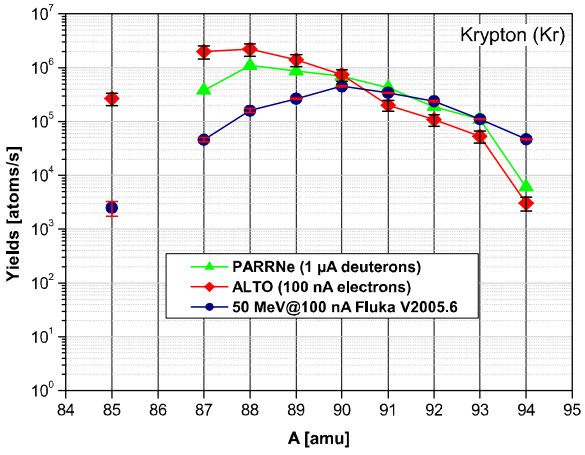

Fig. 7. Isotopic production yield of Kr measured with PARRNe (curve marked with filled triangle-up), ALTO (100 nA) (curve marked with filled rhomb and estimated by FLUKA code (curve marked with filled circle).

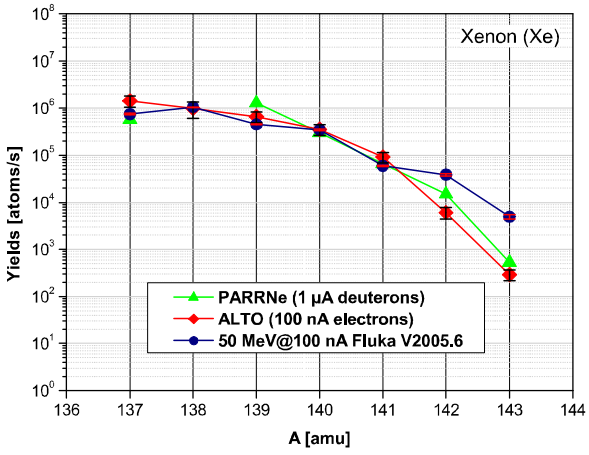

Fig. 8. Isotopic production yield of Xe measured with PARRNe (curve marked with filled triangle-up), ALTO (100 nA) (curve marked with filled rhomb and estimated by FLUKA code (curve marked with filled circle)).

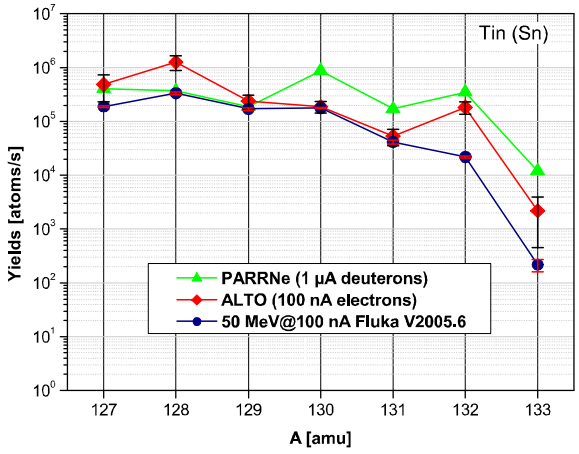

Fig. 9. Isotopic production yield of Sn measured with PARRNe (curve marked with filled triangle-up), ALTO (100 nA) (curve marked with filled rhomb and estimated by FLUKA code (curve marked with filled circle).

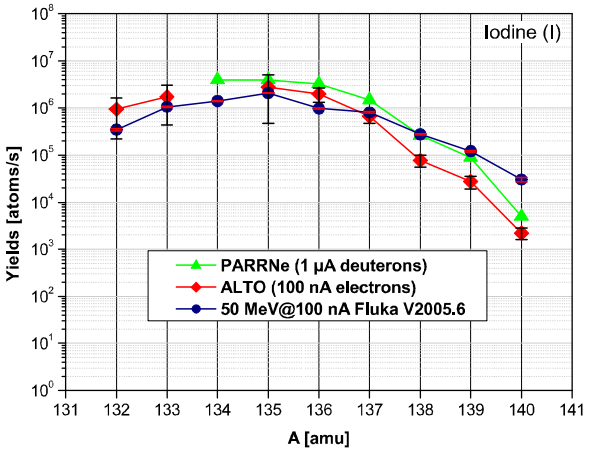

Fig. 10. Isotopic production yield of Iodine measured with PARRNe (curve marked with filled triangle-up), ALTO (100 nA) (curve marked with filled rhomb and estimated by FLUKA code (curve marked with filled circle).

2.2.1.4. Isotopic chain of Iodine. In Fig. 10 results for Iodine are reported. Predicted values by FLUKA simulations reproduce well experimental data of PARRNe and ALTO which are in good agreement too.

3. Conclusions

First experimental results obtained in the first phase of commissioning (100 nA) give results in quite good agreement with calculations based on FLUKA code. Measurement yields at ALTO are comparable to PARRNe ones (26 MeV deuterons, 1 μA) as expected by our calculations.

For short-lived species having negligible accumulated yields, presented simulation results supplying independent production yields are directly comparable to measurements. This validate our benchmarking of the FLUKA code for photofission with 50 MeV electron beam. Thus, we can confirm that production yields with ALTO for 10 μA electron beam will be about two orders of magnitude higher than those obtained at PARRNe for 1 μ*A* deuterons.

Finally, these presented results show in particular the benchmarking of FLUKA for photofission with 50 MeV electron beam and therefore comfort its use for our safety and radioprotection calculations for the design of the target shielding for 10 μA primary electron beam current.

References

[1] F. Clapier et al., Phys. Rev. ST-AB (1998) 013501.
[2] F. Ibrahim et al., Nucl. Phys. A 787 (2007) 110c.
[3] S. Essabaa et al., Nucl. Instr. and Meth. B 204 (2003) 780.
[4] M. Cheikh Mhamed, thèse de l'Université d'Evry Val d'Essonne, 2006, IPNO T 06 05.
[5] L.C. Carraz, I.R. Haldorsen, H.L. Ravn, M. Skarestad, L. Westgaard, Nucl. Instr. and Meth. 148 (1978) 217.
[6] L.C. Carraz, S. Sundell, H.L. Ravn, M. Skarestad, L. Westgaard, Nucl. Instr. and Meth. 158 (1979) 69.
[7] R. Kirchner, E. Roeckl, Nucl. Instr. and Meth. 133 (1976) 187.
[8] R. Kirchner, Nucl. Instr. and Meth. 186 (1981) 275.
[9] S. Sundell, ISOLDE Collaboration, H. Ravn, ISOLDE Collaboration, Nucl. Instr. and Meth. B 70 (1992) 160.
[10] M. Cheikh Mhamed, C. Lau, S. Essabaa, J. Arianer, O. Bajeat, H. Croizet, Rev. Sci. Instr. 77 (2006) 03A702.
[11] C. Lau et al., Rev. Sci. Instr. 77 (2006) 03A706.
[12] K.D.A. Wendt et al., Nucl. Instr. and Meth. B 204 (2003) 325.
[13] A. Fasso, A. Ferrari, J. Ranft, P.R. Sala, CERN-2005-10 (2005), INFN/TC_05/11, SLAC-R-773.
[14] A. Fasso et al., Computing in High Energy and Nuclear Physics 2003 Conference (CHEP2003), La Jolla, CA, USA, March 24-28, 2003, (paper MOMT005), eConf C0303241 (2003), arXiv.hep-ph/0306267.
[15] E. Jacobs, H. Thierens, D. De Frenne, A. De Clerq, P. D'hondt, P. De Gleder, A.J. Deruytter, Phys. Rev. C 19 (1979) 422.
[16] Yu.Ts. Oganessian, S.N. Dmitriev, J. Kliman, O.A. Masslov, G.Ya. Stardub, A.G. Belov, S.P. Tretiakova, Nucl. Phys. A 701 (2002) 87.
[17] C. Lau et al., Nucl. Instr. and Meth. B 204 (2003) 246.
[18] M. Lebois et al., Proceedings of the International Symposium on Exotic Nuclei, Khanty-Mansiysk, Russia, 17-22 July 2006, Yu. E. Penionzhkevich and E.A. Cherepanov Eds, AIP Conf. Proc., Vol912 (2007) 446.
[19] H.L. Ravn et al., Nucl. Instr. and Meth. B 88 (1994) 441.
[20] U.C. Bergmann et al., Nucl. Instr. and Meth. B 204 (2003) 220.
[21] B. Roussière et al., Nucl. Instr. and Meth. B 246 (2006) 288.
[22] G. Rudstam et al., Radiochim. Acta 49 (1990) 155.
[23] <http://ipnweb.in2p3.fr/tandem-alto/alto/accelerateur/production/ALTOion.pdf>.
[24] <http://ie.lbl.gov/fission/238uf.txt>.